

Synergetic Combination of Carbon Xerogels, Graphene Oxide and nano-ZnO for Aqueous and Organic Supercapacitors

Rusbel Coneo-Rodríguez,^[a] Alvaro Yamil Tesio,^[b] Fernando Pablo Cometto,^[c, d]
Gustavo Marcelo Morales,^[a] Gabriel Ángel Planes,^{*[a]} and Alvaro Caballero^{*[e]}

Dedication ∞ Florencia Sofia Podetti in her honor.

Three-dimensional carbon xerogels were synthesised via a facile approach that included the use of ZnO nanostructures both as a templating agent and as a catalyst for resorcinol-formaldehyde resin (R-F) polymerisation simultaneously. Graphene oxide (GO) served as a stabilising agent during the drying and pyrolysis processes, avoiding the collapse of structure and improving the area surface. The method enabled the as-obtained materials to possess optimised 3D porous structures for energy-storage devices, such as wires or spaghetti-like structures. Also, a high BET surface area was obtained ($1661 \text{ m}^2 \text{ g}^{-1}$) without using an additional activating agent. This great surface area improved the specific capacitance compared to materials without GO (358.1 F g^{-1} vs 170.4 F g^{-1}). The carbon-

containing devices derived from resorcinol-formaldehyde resin, GO, and Zn oxide showed better performance than the devices without GO. In particular, the sample that contained 2.5% of GO in the synthesis showed a specific capacitance of 166.6 F g^{-1} at 0.5 A g^{-1} and remained at $\sim 120 \text{ F g}^{-1}$ at 5 A g^{-1} current density. Also, it showed interesting energy density values at 0.5 A g^{-1} (14.8 Wh kg^{-1}) and a power density of 200.7 W kg^{-1} . This reveals that the synthesis process made it possible to obtain composite materials with large surface areas without using a supercritical drying process. The materials can be used in supercapacitor-type devices with high performance in aqueous electrolytes.

Introduction

In recent years, the design and synthesis of materials with more efficient electrochemical performance,^[1] good stability,^[2] and low weight^[3] has attracted considerable attention. Energy storage on a large scale represents a significant challenge to the energy transition because it requires materials capable of being used in batteries and supercapacitors, among other devices, with high energy and power density, long life cycles, and fast charge-discharge rates.^[4] Supercapacitors are especially attractive devices due to their advantages such as fast charge-discharge rate, high power density, and long life cycles.^[4] These devices can be classified into electric double layer capacitors

(EDLCs), pseudocapacitors, and hybrid capacitors according to the energy storage mechanism^[5]. In EDLCs, the capacitance is due to the charge separation at the electrode-electrolyte interface, which is favoured due to the diffusion of ions from the bulk of the electrolyte into the pores of electrodes. This performance is typical of carbonaceous materials. On the other hand, the pseudocapacitors store charge by a faradaic mechanism (oxidation-reduction reactions, and intercalation mechanisms),^[6] while that the hybrid supercapacitors involves a faradaic mechanism storage (battery-like charge storage process) and one EDLC-type.^[7]

The nanostructured carbon materials,^[8] such as carbon nanotubes, graphene, carbon aerogels, etc., are of interest due

[a] R. Coneo-Rodríguez, G. M. Morales, G. Á. Planes

Facultad de Ciencias Exactas Fisicoquímicas y Naturales, Instituto de Investigaciones en Tecnologías Energéticas y Materiales Avanzados (IITEMA), Universidad Nacional de Río Cuarto-CONICET, Ruta Nac. 36, Km 601, Río Cuarto, Córdoba, Argentina
E-mail: gplanes@exa.unrc.edu.ar

[b] A. Y. Tesio

Centro de Desarrollo Tecnológico General Savio, Centro de Investigación y Desarrollo en Materiales Avanzados y Almacenamiento de Energía de Jujuy-CIDMEJu (CONICET-Universidad Nacional de Jujuy), Palpalá, Jujuy 4612, Argentina

[c] F. P. Cometto

Universidad Nacional de Córdoba, Facultad de Ciencias Químicas, Departamento de Fisicoquímica, X5000HUA Córdoba, Argentina

[d] F. P. Cometto

Consejo Nacional de Investigaciones Científicas y Técnicas, CONICET, Instituto de Investigaciones en Físico-Química de Córdoba (INFIQC), X5000HUA, Córdoba, Argentina

[e] A. Caballero

Dpto. Química Inorgánica e Ingeniería Química, Instituto Químico para la Energía y el Medioambiente (IQUEMA), Universidad de Córdoba, 14071 Córdoba, Spain
E-mail: alvaro.caballero@uco.es

Supporting information for this article is available on the WWW under <https://doi.org/10.1002/batt.202400502>

© 2024 The Authors. Batteries & Supercaps published by Wiley-VCH GmbH. This is an open access article under the terms of the Creative Commons Attribution Non-Commercial License, which permits use, distribution and reproduction in any medium, provided the original work is properly cited and is not used for commercial purposes.

to their large surface area, good conductivity, and good chemical and thermal stability.^[9] For these reasons, the materials have been employed successfully in energy storage and generation devices.^[10] However, the synthesis processes are expensive and difficult in most cases, due to the use and removal of hard templates^[11,12] or the use of supercritical process. Researchers are focussing their attention on new synthetic strategies^[13] that allow obtaining carbon materials with better properties and can be applied in energetic systems with high performance. According to the previous commentaries, several synthetic strategies have been used to obtain nanostructured carbon materials. One approach employs templates such as surfactants or inorganic nanoparticles (NPs) in combination with resin precursors based on organic polymers. However, in these synthesis processes is necessary to use catalysts. Using NPs or surfactants as template agents (hard or soft) is one of the most common techniques in synthesising carbon nanostructures.^[14,15] This is due to their multiple advantages. For example, they can maintain their microstructures during the synthesis processes.^[16]

On the other hand, the NPs based on inorganic oxides, such as SiO_2 ,^[17] Fe_2O_3 ,^[18] TiO_2 ,^[19] etc., have been successfully employed in the synthesis of porous carbons. These materials are characterised by having a large surface area and efficient ion transport/diffusion for applications in fuel cells, batteries, and supercapacitor electrodes. In this work, we propose ZnO as a hard template for a new synthetic strategy. Zinc oxide is interesting because it is a multi-use material that has been utilised in a multiplicity of applications such as catalysts, antibacterial agents, and photo-catalysts.^[20] Also, it is characterised as having excellent optical properties,^[21] low cost, environmental friendliness^[22] and a facile synthesis.^[23] The use of ZnO as a template in nanostructured carbon synthesis has been reported in several scientific publications.^[23–25] However, some authors highlight the ability of these oxides to act as a template, their additional activation function (formation of micropores),^[23] and their graphitisation catalysis effect.^[26] In order to design new materials, we propose using facilely synthesised ZnO nanostructures as templates and catalysts in the polycondensation reaction of resorcinol-formaldehyde (RF) resin, as carbon precursor. This new procedure avoids using the acidic or basic catalyst agents commonly employed in RF polymerisation.

The RF polymers have been used as precursors of highly porous activated carbons^[27] and allow obtaining materials with different morphologies and structural properties according to the synthesis conditions used. In the case of carbon aerogels based on RF, it was observed that their surface properties depend on the type of catalyst employed,^[28] the initial conditions of synthesis, and also on the drying techniques.^[29] However, the drying step is one of the most critical stages because the structure can collapse during the elimination of water from RF hydrogel (to obtain a solid RF gel), affecting the surface area and pore size of the final material. The organic gel tends to collapse during drying because its gel networks are too weak to withstand the capillary pressure built up in the pore walls.^[11]

In order to avoid this collapse in the structure, techniques such as drying in an inert atmosphere, freeze-drying, and supercritical extraction have been used.^[29] Nevertheless, another alternative uses graphene oxide as a stabilising agent in RF hydrogel. Although their use has been reported in combination with other materials, such as CNT, carbon fibres or spheres, etc. To the best of our knowledge, the use of GO in combination with RF resin and ZnO for synthesizing carbon xerogels has not been reported.^[30]

In this work, we report a new synthetic strategy for obtaining carbon xerogels through the combination of RF resin, ZnO nanostructures, and GO.^[31] The combination of these materials allowed the design and preparation of novel micro/mesoporous carbons using ZnO as a template, GO as a stabilising agent during the drying of hydrogel, and RF as the carbon source. In addition, we present the characterization and performance of the materials for their application as advanced electrodes in electrochemical supercapacitors. By varying the percentage of GO in the synthesis, different samples were obtained while the pyrolysis conditions were constant for all samples. The performance of the synthesised carbon xerogels as electrochemical supercapacitors was studied using aqueous H_2SO_4 and organic LiPF_6 -based solutions as electrolytes. In the case of the H_2SO_4 solution, a predominant double-layer capacitive behaviour was observed for all samples. This showed the influence of the textural properties of carbon xerogel on the capacitance values of the system. When used as electrodes, the materials showed good capacitance retention, high specific capacitance values, and high stability.

Results and Discussion

Structural and Chemical Characteristics

The proposed synthesis procedure intended to obtain nanostructured carbon xerogels with high surface area by a combination of graphene oxide (GO), zinc oxide (ZnO), and resorcinol-formaldehyde (RF) resin as a carbon precursor. In this process, using a simple one-step pyrolysis method, the ZnO nanostructures (wires or belts type) act as a template and catalyst agent simultaneously and GO as a stabiliser agent for the 3D xerogels. In order to evaluate the materials obtained by this synthetic process, extensive structural, chemical, physical, and morphologic characterisations were carried out (See schematic of the synthesis process in Figure 1).

With regard to structural characterisation, the X-ray patterns of the synthesised materials showed two broad diffraction bands at 2θ values, one between 25–26° and another around 44° (Figure 2a). These bands are usually attributable to 002 and 100 planes, respectively, which corresponds to reflections of graphitic carbon (JCPDS card no. 41–1487).^[8,32] However, the broad band around of 44° can be formed for several planes, such as the (100), (010), and (101) planes.^[33] The XRD experiments confirmed the presence of crystalline ZnO (zincite) in all cases. The diffraction peaks located at 31.7°, 34.4°, 36.2°, 47.4°, 56.5°, 62.8°, 68°, and 69.31° correspond to the (100), (001),



Figure 1. Schematic diagram of synthesis process and preparation of the 3D carbon xerogels.

(101), (102), (110), (103), (112), and (201) planes of hexagonal structured ZnO, in agreement with the JCPDS card no 89-1397.^[34] The presence of ZnO is expected due to its use as a template in the synthesis process. On the other hand, the GO added during the synthesis is reduced (rGO) as a consequence of thermic treatment in an inert atmosphere. This can be confirmed by XRD results due to the absence of a diffraction peak at around 10.27° , a characteristic of GO,^[35,36] which was simultaneously reduced during the transformation of the polymer in carbon.

The morphological properties of the synthesized porous materials, such as specific surface area (SSA) and porosity were evaluated by nitrogen adsorption-desorption isotherms applying the Brunauer–Emmett–Teller (BET) method (Figure 2b and c). The results shown that the materials have high SSA: 693, 1661 and $992 \text{ m}^2 \text{ g}^{-1}$ for CRFZn, CRFZn-GO1, CRFZn-GO2 and CRFZn-GO3 respectively (Table 1). The samples present a combination of adsorption-desorption isotherms type I and IV, which can be associated with the presence of different pore sizes or hierarchical porous structure.^[26,37] In addition, a hysteresis loop at a relative pressure (p/p_0) of 0.40–0.99 can be observed and this confirms the presence of meso and macroporous.^[38]

The larger surface area is obtained for the CRFZn-GO2 sample, which is in agreement with what is observed in Figure 2b and c and assigned to the contribution from micro and mesoporous in comparison with the other samples.

Three well defined regions can be observed in the pore size distribution curves (See Figures 2c and S1), where the difference between synthesized materials is noted in the micro and

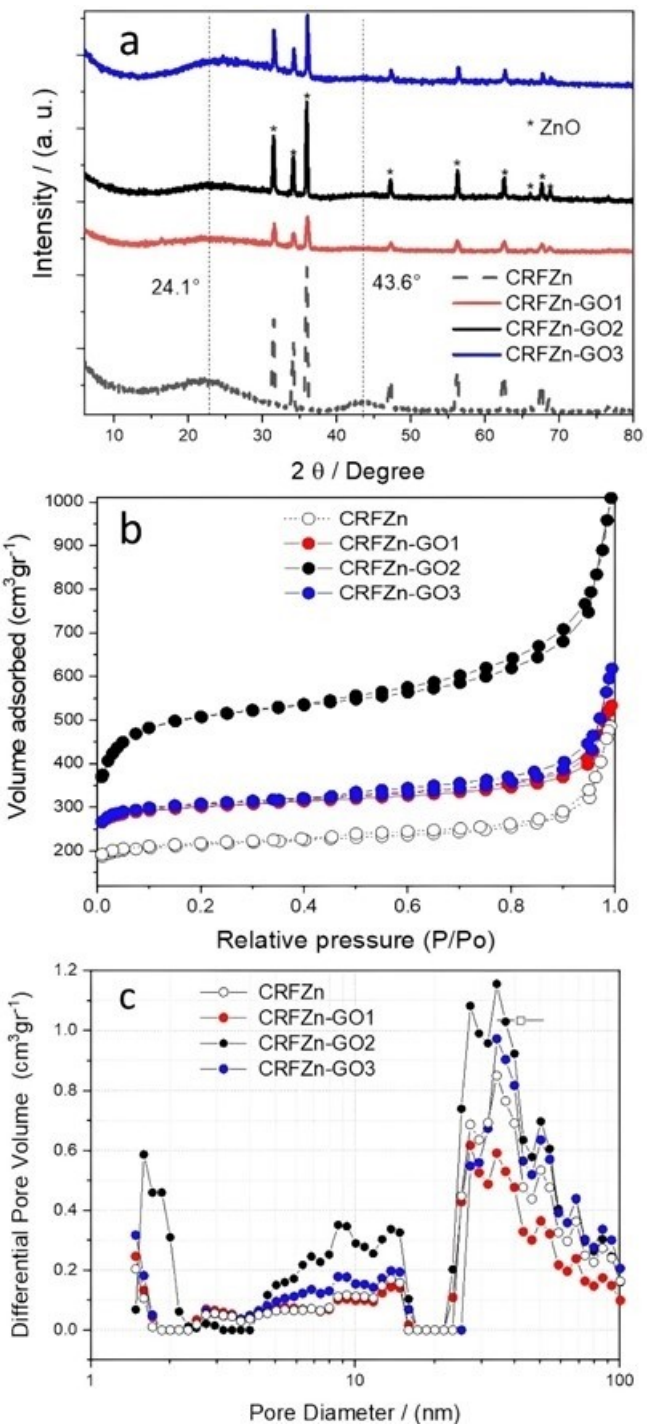


Figure 2. (a) XRD patterns of carbon xerogels based in resorcinol-formaldehyde with GO and ZnO after pyrolysed at 800°C in an inert atmosphere, (b) Nitrogen adsorption/desorption isotherms, and (c) Differential pore volume ($\text{cm}^3 \text{ g}^{-1}$) vs pore diameter of carbon xerogels.

mesoporous regions, being the sample CRFZn-GO2 the one with the highest total pore volume (See Table 1 and Figure S2 in SI).

In Table 1, it is possible to observe the differences in the textural properties between the samples synthesized and the

Table 1. Textural properties of the CRFZn-based samples.^[a]

	CRFZn	CRFZn-GO1	CRFZn-GO2	CRFZn-GO3
BET Surface Area (S_{BET})	693 m ² .g ⁻¹	971 m ² .g ⁻¹	1661 m ² .g ⁻¹	992 m ² .g ⁻¹
Micropore Area (S_{Micro})	540 m ² .g ⁻¹	784 m ² .g ⁻¹	1168 m ² .g ⁻¹	801 m ² .g ⁻¹
Total pore volume (VT)	0.752 cm ³ .g ⁻¹	0.825 cm ³ .g ⁻¹	1.561 cm ³ .g ⁻¹	0.956 cm ³ .g ⁻¹
Micropore volume	0.264 cm ³ .g ⁻¹	0.384 cm ³ .g ⁻¹	0.569 cm ³ .g ⁻¹	0.392 cm ³ .g ⁻¹

[a] Micropore data calculated by t-plot method.

influence of GO in the characteristics final of carbon material in terms of surface area, micropore area and total pore volume.

A detailed XPS analysis was performed to study the composition and evolution of the chemical environment of the different species after thermal treatment. XPS is a powerful technique that provides qualitative and quantitative information about the chemical nature of the surface of a sample.^[39] Analysing the survey spectra of the different samples (Figure S3) shows that the only (detectable) elements present are C, O, and Zn. The relative elemental atomic percentages of C, O, and Zn were calculated and summarised in Table 2.

From Table 1, it can be noted that the total amount of C, O, and Zn atoms detected by XPS analysis varies from sample to sample. At first sight, it can be observed that the compositions of CRFZn-GO1 and CRFZn-GO2 samples are quite similar. Nevertheless, the most remarkable difference is the high amount of O atoms in the sample without GO. As we shall describe later, it seems that graphitisation in this sample is not as complete as in the samples with the GO additive. It is observed that fewer carbon atoms are present within the volume that XPS can detect (approximately 7 Å) in the CRFZn sample. This behaviour is associated with the higher amount of precursor carbon employed in the CRFZn-GOx samples compared to the CRFZn. On the other hand, samples with GO as an additive show similar compositions of C and O. However, the amount of Zn in the CRFZn-GO3 is surprisingly higher (1.05 % vs 0.38–0.33 %). This difference could be attributed to a decrease in the inelastic scattering of the ejected Zn photoelectrons due to the increased porosity of samples with higher GO content. Also, the percentage of C decreases with increasing GO in the synthesis, and this behaviour is accompanied by an increase in the percentage of O, which is associated with oxygen-containing functional groups provided for the GO due to an insufficient reduction process after pyrolysis.^[40,41]

Further analyses were performed comparing the C 1s, O 1s, and Zn 2p spectra recorded for CRFZn, CRFZn-GO1, CRFZn-GO2, and CRFZn-GO3 samples (Figure 3). From the best fitting

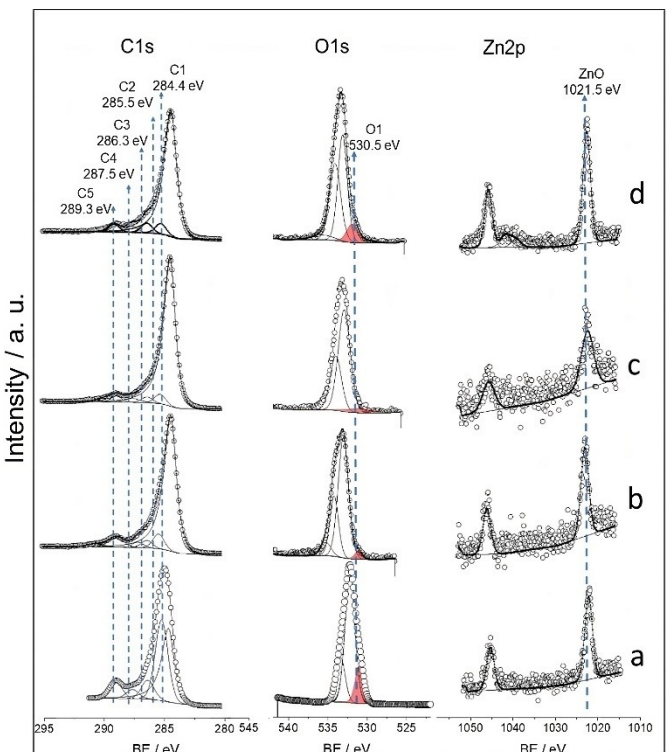


Figure 3. (a) XRD patterns XPS spectra of carbon xerogels in the C1s, O1s, and Zn2p regions. (a) CRFZn, (b) CRFZn-GO1, (c) CRFZn-GO2 and (d) CRFZn-GO3.

procedure of C 1s spectra, five different components can be distinguished: C1 at 284.4 eV, attributed to sp² carbon atoms from graphitic carbon, C2 at 285.5 eV to C–O in defective sp² C and/or C–OH (from incomplete resorcinol decomposition), C3 at 286.3 eV related to O–C–O, C4 for C=O species, and C5 attributed to carboxylic species O–C=O, respectively (Figure 3). As mentioned above, according to the O content calculated from surveys, it seems that carbonisation is highly favoured by the presence of GO in the synthetic process. Component C1 is

Table 2. Atomic percentages (%At) of C, O, and Zn obtained after the analysis of C1s, O1s, and Zn2p components in XPS surveys. Individual percentages of each atom in its different chemical environment and specific information are in Figure S2.

	CRFZn	CRFZn-GO1	CRFZn-GO2	CRFZn-GO3
C	74 ± 2 %	90 ± 2 %	88 ± 1 %	83 ± 1 %
O	26 ± 1 %	10 ± 2 %	11 ± 1 %	16 ± 1 %
Zn	0.41 ± 0.03 %	0.38 ± 0.02 %	0.33 ± 0.03 %	1.05 ± 0.05 %

the main feature in CRFZn-GO1-3 samples, whereas it is a secondary peak in CRFZn samples. That means that GO not only participates as a template for pore generation but also could catalyse the graphitisation process in combination with the ZnO.

Figure 3 shows the spectra of the samples in the O 1s and Zn 2p regions. Analysis of the O 1s spectra is not straightforward because this region (530.5–534.5 eV) is congested with signals originating from organic compounds containing oxygen atoms, hydroxyls, and water molecules, in most cases. Nevertheless, we can identify 4 well-defined peaks: O1 at 530.5 eV attributed to Zn–O_{vac} and Zn–O–C bonds,^[42,43] whereas O2 at 531.8 eV, O3 at 532.5 eV, and O4 at 534.5 eV are attributed to C–O, C=O/C–OH, and carbonates, respectively. The assignment of O1 is also confirmed in Figure 3, and the characteristic Zn2p doublet at around 1021.5 eV (and 1045.6 eV) is assigned to oxidised Zn species.^[44] Summarising, according to the XPS measurements, it can be observed that samples containing GO as an additive in the synthetic process present a higher degree of graphitisation in comparison to samples without GO.

Additional information on the carbonaceous materials synthesised in this work is revealed by the Raman spectra (See Figure 4a). In all cases, the Raman spectrum exhibits a strong peak at 1591 cm⁻¹ corresponding to the band G (E_{2g} symmetry) and another peak centred at approximately 1339 cm⁻¹, corresponding to Band D (mode A_{1g} symmetry) of carbon.^[45] A band

of low intensity is observed between 2300 cm⁻¹ and 3200 cm⁻¹, which can be attributed to the 2D band, which is characteristic of graphitic materials.^[46] However, in this 2D band, three signals can be differentiated through deconvolution processing (Figure S4). Also, the low definition in these bands would be related to the presence of disordered carbon, according to previous work.^[47] On the other hand, the I_D/I_G ratio (intensity ratio values) was calculated and plotted vs % GO employed in the synthesis process (Figure S5). In all samples, the I_D/I_G ratio values observed were less than 1. However, these values were higher for the samples CRFZn-GO1, CRFZn-GO2, and CRFZn-GO3 containing GO (I_D/I_G=0.876, 0.914, and 0.885, respectively) in comparison with CRFZn sample (0.868) without GO. This increase in the I_D/I_G values could be associated with an increase in the percentage of structural defects,^[48] being higher in CRFZn-GO2 sample as a consequence of the RF/GO ratio used in the synthesis.

In order to study the influence of GO on the thermal stability of the carbon materials obtained, thermogravimetric analysis (TGA) was performed, and the results are shown in Figure 4b. A significant weight loss can be observed in the samples containing GO compared to CRFZn, without GO. This weight loss at low temperatures is characteristic of partially reduced GO samples; starting between 35 and 60°C and reaching a plateau around 100°C and it is associated with dehydration. For temperatures greater than 100°C, the mass loss continues to decrease slowly as a consequence of the evolution of H₂O and CO₂, resulting from the removal of remaining oxygen functional groups.^[49] The presence of these surface groups is due to the fact that GO is not completely reduced, as was observed by XPS experiments. Note that the observed behaviour in this temperature range is not seen in the CRFZn sample. The minimal mass loss observed in CRFZn up to 500°C implies the presence of few original functional groups in this sample. The thermal decomposition of xerogel carbons starts in the vicinity of 450°C, with a notable weight loss observed around 550°C. This mass lost is associated with carbon combustion (thermal oxidation of carbon)^[50,51] and represents around 80–90% of the total mass of the composite.

In order to corroborate the morphology of the synthesised carbon materials, scanning electron microscopy (SEM) was carried out, and the images are shown in Figure 5. The materials exhibit characteristic morphologies attributed to the skeletal contributions of ZnO on the nanoscale, as well as the inclusion of RF in the synthesis process. Figure S6 shows a macroscopic monolithic spaghetti-type structure of interlaced wires. In addition, changes in the structure can be observed when the GO is involucrate in the process. Figure 5a shows a SEM image of the xerogel without GO, where elongated wire-like or spaghetti-like network decorated with carbonaceous material can be observed (Figure S7). However, when GO is present in the synthesis process (Figure 5b and c), the spaces between the microstructures are further apart from one another. It is believed that the presence of GO stabilizes the gel during drying (before pyrolysis), preventing the collapse of its microstructure and providing structural strength to the matrix.^[52] This observation is consistent with the changes in the surface area measured through BET analysis when GO is present in the

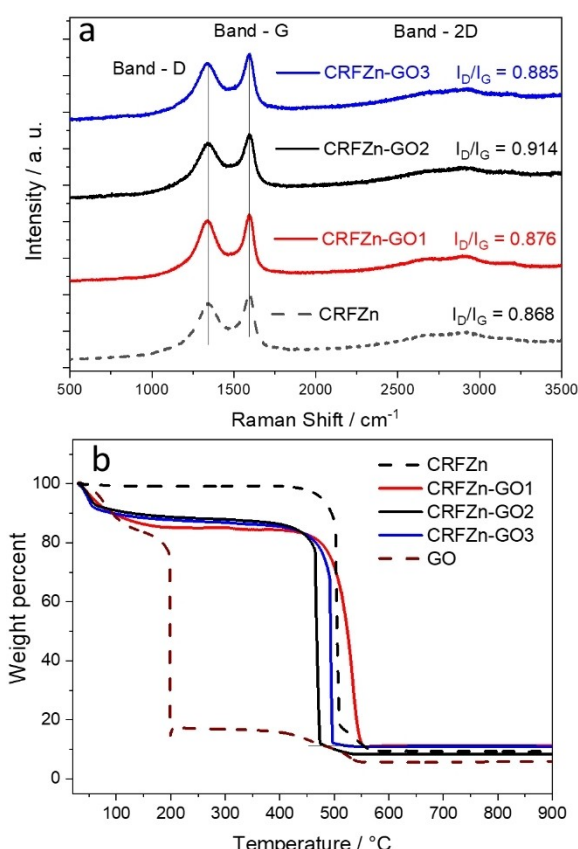


Figure 4. (a) Raman spectra of carbon xerogels and (b) TG measurements of carbon xerogel samples.

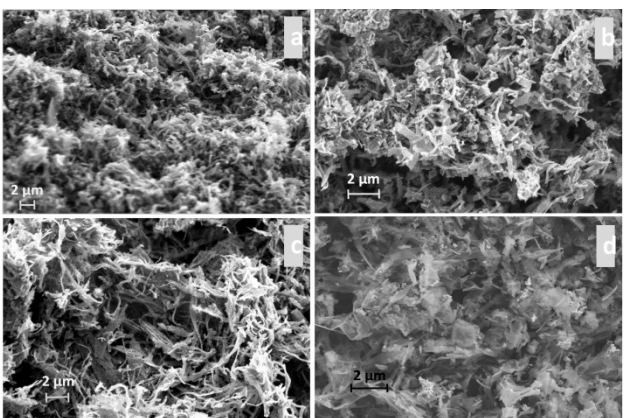


Figure 5. SEM images of carbon xerogels at different magnifications are presented. (a) CRFZn, (b) CRFZn-GO1, (c) CRFZn-GO2, and (d) CRFZn-GO3.

appropriate proportion (See Table 1 and Figure 2c). Figure 5d displays the carbon xerogels synthesized with the highest GO proportion in their composition (5.0%). In this case, the sample exhibits a structure primarily composed of sheets associated with GO, sharing characteristics similar to the samples obtained using GO and RF without ZnO. (Figure S8).

The wire-like or spaghetti-like nanostructures are observed in all cases and are a result of the use of ZnO as a template and catalyst. The impact of the absence of these wire-like structures in the composite is observed in samples obtained using only GO and RF (See Figure S8), resulting in a compact material (Figure 5a). This indicates the importance of structured ZnO as a template for obtaining these 3D carbonaceous systems. On the other hand, the presence of macropores (void spaces between the nanostructure) is more appreciable in the samples CRFZn-

GO1, CRFZn-GO2, and CRFZn-GO3 compared to CRFZn. This correlates with the results obtained by BET analysis and can be associated with the stabilization effect induced by the presence of GO, preventing or minimizing the collapse of the 3D structure during the drying of the organogels.^[53] However, when the amount of GO in the synthesis is increased beyond a certain value (samples CRFZn-GO3), the GO sheets begin to spontaneously stack, due to this increased their interfacial friction, affecting the final structure of the obtained materials.^[54] Finally, the SEM-EDS elemental mapping shows the presence of zinc and oxygen atoms dispersed in the carbon matrix (Figures S9 and S10).

X-ray mapping, along with XPS, was conducted to demonstrate the elemental content of the synthesized carbon xerogels. The results suggest that the reported synthetic method allows for the design of 3D carbon materials with morphological and surface properties that can provide reactive sites for charge-transfer reactions and facilitate the transport of electrons and electrolytes. This finding indicates potential applications in electrochemical supercapacitors.

To test this hypothesis, electrochemical capacitors were assembled and electrochemically tested. The electrochemical characterization of the carbon xerogels was conducted in a three-electrode configuration using 0.5 M sulfuric acid as the aqueous electrolyte. Figure 6a presents the cyclic voltammetry (CV) studies of CRFZn, CRFZn-GO1, CRFZn-GO2, and CRFZn-GO3 samples at a sweep rate of 10 mVs⁻¹. In these experimental conditions, it is possible to see that all the CV curves showed approximately symmetrical rectangular shapes, which indicates a near-ideal double-layer capacitance behaviour.^[55] However, broad peaks observed at around 0.3–0.35 V suggest pseudocapacitive contributions that are probably associated with the oxygen-functionalized group present on the carbon surface.^[56,57]

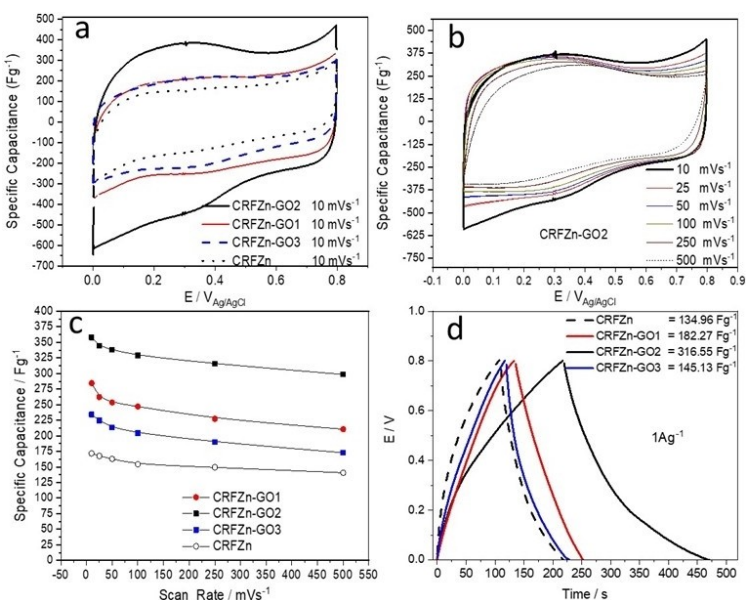


Figure 6. Electrochemical performance. (a) CV curves at 10 mVs⁻¹ for CRFZn, CRFZn-GO1, CRFZn-GO2, and CRFZn-GO3, (b) CV curves of CRFZn-GO2 at various scan rates, (c) specific capacitance at various scan rates of CRFZn, CRFZn-GO1, CRFZn-GO2, and CRFZn-GO3, and (d) Galvanostatic discharge-charge curves at a current density of 1 A g⁻¹. Three electrode cell with 0.5 M H₂SO₄ and Ag/AgCl as the reference electrode.

The origin of the stored charge was characterized by analysing the CV data at different sweep rates; follows a power-law correlation of the current (i) with the sweep rate (v), see Equations (6) and (7) in SI. The b-values determined from the slope of the plot of $\log i$ vs. $\log v$ give values close to 1 for all synthesised materials (Figure S11), indicating a surface-controlled charge storage mechanism predominately.^[58]

The capacitive and diffusive contributions for all systems were calculated according to Equation (8) (see SI) and the values obtained at different scan rates can be observed in detail in Table S1 and represented in Figure S12. It was observed that as the scan rate increased, the contribution of the capacitive process vs the diffusion process increased, due to this higher scan rate, it surpasses the diffusion rate causing a loss of linearity making the slope smaller.^[59]

The CV studies for all materials obtained, measured at different scan rates from 10 to 500 mVs⁻¹ (Figure S13), also showed quasi-rectangular CV profiles in all cases. This fact demonstrates an efficient and fast charge transfer and suggests a fast double layer charge/discharge process too.^[60,61] Considering that charge storage in these materials involves a surface process, it is expected that the material with the highest specific surface area will exhibit the best capacitive performance. In Figure 6b shows the CV curves at different scan rates for the CRFZn-GO2 electrode, allowing the influence of this parameter on the behaviour of the electrode to be observed. The electrochemical response maintained the same shape even at the highest tested scan rate (500 mVs⁻¹), indicating low polarization resistance and a fast response for ion and electron transport.^[4] The specific capacitances calculated at different scan rates for all synthesized materials are compared in Figure 6c. As expected, it is observed that the sample CRFZn-GO2 (358.1 Fg⁻¹) exhibited a higher specific capacitance than CRFZn-GO1, CRFZn-GO3, and CRFZn (284.6, 234.3, and 170.4 Fg⁻¹, respectively). Thus, at a low scan rate, the specific capacitance of CRFZn-GO2 is about two times higher than that of CRFZn. This result is in agreement with the surface area data obtained by BET analysis (1661 m²g⁻¹ vs 692 m²g⁻¹). As reported previously for other carbon xerogels, the capacitance can be correlated to the amount of micro and mesopores in the samples (Figure S14).^[62] Figure 6c also indicates that the specific capacitance decreases moderately as the scan rate increases. These results indicate that at relatively high scan rates, most of the surface area and pores of the 3D carbon electrodes are accessible to the electrolyte ions.^[63] In accordance with the literature, at a low scan rate, the ions have enough time to penetrate the micropores and be efficiently adsorbed into them. This results in smaller charge separation distances between the ion centers, causing a significant increase in capacitance.^[63,64]

The supercapacitive performance of the synthesized carbon xerogels was compared through galvanostatic charge-discharge (GCD) measurements at a current density of 1 Ag⁻¹ (Figure 6d) and the efficiency obtained for each material was 98.34%, 94.36%, 88.25% and 97.43% for CRFZn, CRFZn-GO1, CRFZn-GO2, and CRFZn-GO3 respectively. The specific capacitance values obtained are in line with the results obtained by

CV experiments. This result demonstrates that the obtained materials could be employed in the development of electrochemical devices. Following the trend observed in the CV experiments, the highest capacitance was obtained for CRFZn-GO2 (316.5 Fg⁻¹), and the lowest was for CRFZn (135.0 Fg⁻¹). The enhanced electrochemical performance of carbon xerogels containing GO can be attributed to the synergistic effects of the carbon sheets (the stabilizing effect of GO in RF gels/contribution in specific surface area) and the templating agent (ZnO) employed in the synthesis process. In order to obtain more detailed information about the electrode response, impedance spectroscopic analysis (EIS) was performed on the samples. The Nyquist plot measured in the frequency range of 0.01 Hz to 100 k Hz are shown in Figure S15. The response in the high frequency region shows a deformed semicircle, while in the low frequency region it approaches a vertical line. The behaviour at high frequencies shows a lower internal resistance and faster charge transfer, while the line at low frequencies is almost perpendicular to the x-axis, indicating an ideal capacitance behaviour with fast ion transfer in the electrolyte.^[65]

GCD curves were measured at current densities ranging from 0.5 to 5.0 Ag⁻¹ (Figure 7a), and the corresponding specific capacitance values can be observed in Figure 7b. The capacitance for CRFZn-GO2 were 394.3, 343.1, 314.0, 226.0, and 212.6 Fg⁻¹ at 0.5, 0.75, 1.0, 2.0, and 5.0 Ag⁻¹, respectively. As discussed above and in agreement with the CV results,

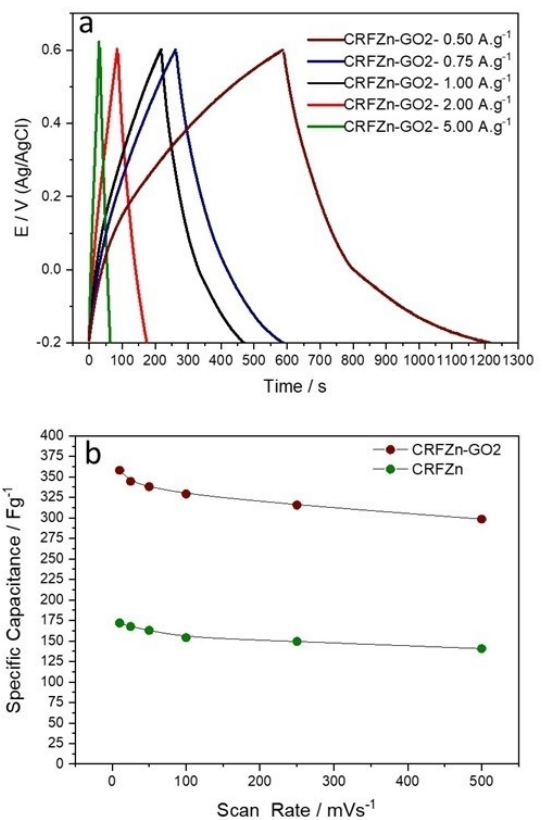


Figure 7. (a) Galvanostatic charge-discharge curves CRFZn-GO2 carbon at different density currents. (b) Comparison of specific capacitance between CRFZn-GO2 and CRFZn electrodes in a three-electrode cell with 0.5 M H₂SO₄ electrolyte and Ag/AgCl reference electrode.

capacitance values decrease with an increase in current density. The results indicate that the synthesized carbon xerogel materials are suitable for supercapacitor applications, as the values obtained in terms of specific capacitance are comparable to those recently reported by other authors (See Table S2). However, we focused our studies only on CRFZn-GO₂ by building a symmetrical supercapacitor.

Symmetric Supercapacitor Performance

The supercapacitor devices were constructed using two electrodes with CRFZn-GO₂ as the active material and were tested in a 0.5 M aqueous H₂SO₄ electrolyte (Figure 8a). To analyse the electrochemical performance of the symmetric device, GCD curves at different current densities were conducted. It can be observed that the device exhibits good electrochemical reversibility with an insignificant IR drop, indicating high electrical conductivity.^[4,66] By analysing the slope of the voltage drop over time, an equivalent series resistance (ESR) of 0.16 Ω was calculated. GCD experiments were performed using different current densities of 0.5, 1.0, 2.0, and 5.0 A g⁻¹, which resulted in specific capacitances of 166.6, 156.3, 149.2, and 119.7 F g⁻¹, respectively. The capacitance retention, calculated after 3000 cycles at 0.5 A g⁻¹, was 97% of the initial capacitance (161.6 F g⁻¹) and efficiency Coulombic efficiency varied between 96.5 and 90% during operation (See S16). These results indicate both high capacitance and a high retention rate after long-term

cycling (Figure 8b). The observed excellent rate capability can be attributed to the porous 3D structure of the carbon material, coupled with the contribution of GO. This contribution enhances the gel stability before pyrolysis, preventing collapse during the drying process, and improves the conductivity of carbon xerogels.^[67]

Utilizing the values of the initial specific capacitance, the obtained energy density at 0.5 A g⁻¹ was 14.8 Wh kg⁻¹, and the power density was 200.7 W kg⁻¹ (refer to energy density values in Figure S17). These values of energy density exceed those reported for a commercial device (8 Wh kg⁻¹)^[8] and are comparable to values reported for an asymmetrical device (19.1 Wh kg⁻¹)^[68] and for a device that employed bio-waste as the active material (12.5 Wh kg⁻¹).^[69] On the other hand, it can be observed that at 1.0 A g⁻¹, the energy and power density were 13.8 Wh kg⁻¹ and 400.7 W kg⁻¹, respectively, while that at 2.0 A g⁻¹ current density, the energy and power density were 13.2 Wh kg⁻¹ and 801 W kg⁻¹. Therefore, we can highlight the low loss of energy density at 2.0 A g⁻¹, which represents 10% of initial energy density.

The variation of specific capacitance of the device with the current density is shown in Figure 8c. It is found that when the current density is increased from 0.5 to 5 A g⁻¹, the capacitance decreases from 166 to 120 F g⁻¹, representing a capacitance retention of approximately 72%. However, at 2.0 A g⁻¹, the capacitance retention was 90%, aligning with the low loss of energy density observed in this device.

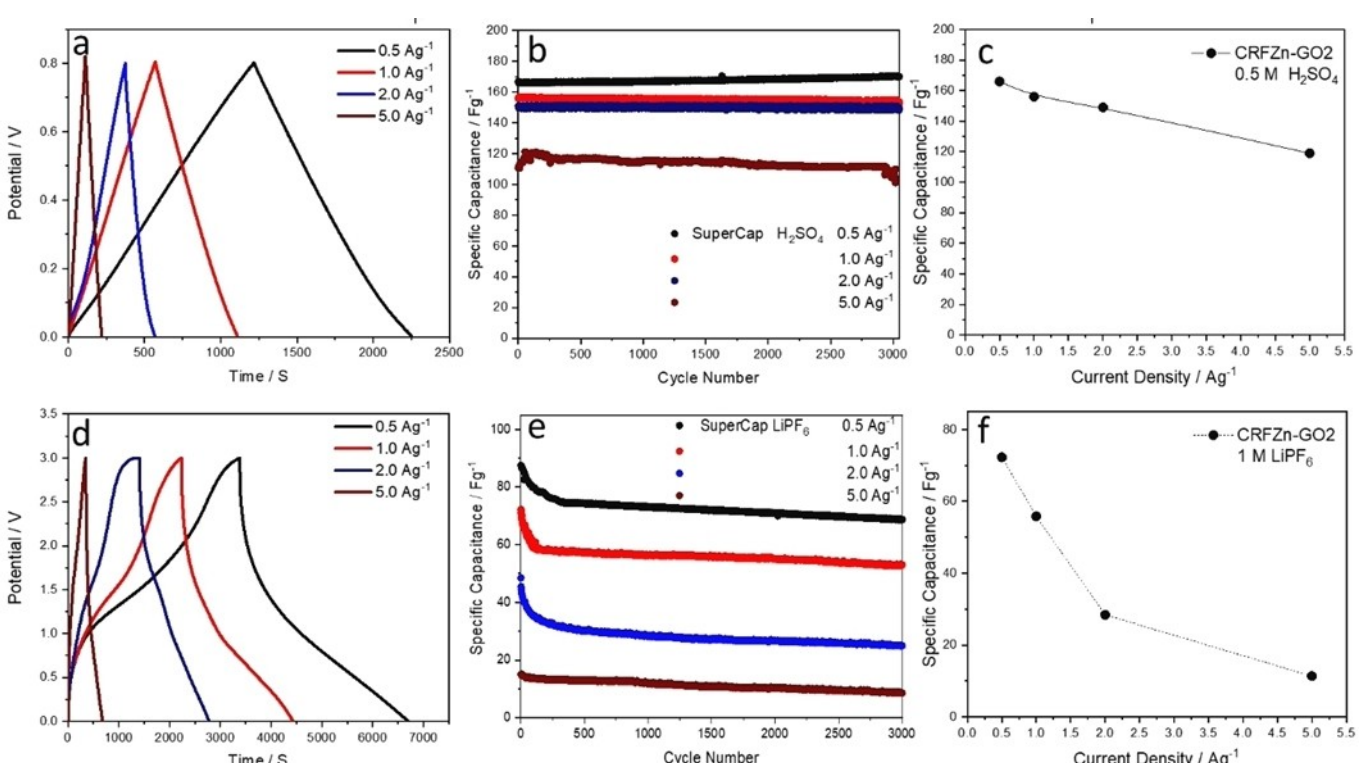


Figure 8. (a) Galvanostatic charge–discharge curves for the device assembled using electrodes of CRFZn-GO₂ in 0.5 M H₂SO₄, (b) cycling stability at different currents densities and (c) specific capacitance. (d) Galvanostatic charge–discharge curves for the device assembled using electrodes of CRFZn-GO₂ in 1 M LiPF₆/ethylene carbonate-diethyl carbonate, (e) cycling stability at different currents densities and (f) specific capacitance.

To expand the possible applications in energy storage, the performance of the device in organic LiPF₆-based electrolytes was explored. The organic electrolytes present advantages compared with aqueous ones; they allow the device to operate in a higher voltage window, achieve lower self-discharge rates, and are suitable for high-energy-density applications, among other potential benefits.^[70] The results reveal specific capacitance values of 72.25, 55.81, 28.42, and 11.37 Fg⁻¹ at current densities of 0.5, 1.0, 2.0, and 5.0 Ag⁻¹, respectively (Figure 8d and e).

In Figure 8e is observed a rapid decrease in specific capacity during the first few cycles at 0.5, 1.0, and 2.0 Ag⁻¹. This performance may be related to the incorporation/intercalation of anions in the active material, which can cause some deterioration of the carbon structure, including from the initial cycles, as it has been reported for other authors.^[71]

These values obtained are lower than those calculated for aqueous systems due to the larger size of Li⁺ and PF₆⁻ ions (0.79 nm for both cation and anion^[72]), in comparison to H⁺ and SO₄²⁻ ions (0.115 nm and 0.379 nm, respectively). The smaller size of the latter ions allows for the accommodation of more ions in the micropores, leading to an increase in specific capacitance.^[73] However, a higher energy density (90.3 Wh kg⁻¹) and power density (750 W kg⁻¹) were obtained using non-aqueous electrolyte compared to the device in aqueous electrolyte. The comparison of the performance of both devices is shown in the Ragone plots in Figures 9 and S17.

The CRFZn-GO2 device exhibits higher power and energy density in the 1 M LiPF₆ electrolyte due to the broader potential window, compensating for the lower capacity compared to aqueous electrolytes. These values of power and density are in the range of values reported for carbon-based biomass^[74] and present a higher energy power density than other graphene materials used in advanced Li-ion hybrid supercapacitors.^[75] The data demonstrate the possibility of utilizing the materials synthesized by employing GO, ZnO, and RF resin in super-

capacitors based on both aqueous electrolytes and lithium-ion electrolytes.

The results showed that it was possible to fabricate new carbon materials by combining structures capable of acting as a template agent and catalyst of RF polymerisation, using GO as a possible stabilisation agent of the hydrogel carbon precursor during the drying and pyrolysis processes. In addition, the significant surface area observed for these materials is related to ZnO, as it acts as both a template and a catalyst, allowing the nanostructured materials to be obtained after pyrolysis. Also, it has been reported to be an activating agent by other authors. Which show its additional activating function.^[23] The combination of ZnO, RF and GO allows obtaining carbon xerogels with a large surface area and high values of specific capacitance. In this work, we demonstrated a simple method that combines materials with specific functions for the design of 3D carbon nanostructures, aiming to obtain advanced materials for applications in energy storage devices such as supercapacitors.

Conclusions

In summary, nanostructured 3D carbon xerogels were obtained by a new, simple and reproducible synthetic approach which consists of using ZnO as a templating agent and catalyst for the polymerisation of R-F resin. The ZnO is used in combination with GO that acts as a stabilising agent of R-F gels to avoid structure collapse during the drying process. This method did not require a supercritical process, which is more inexpensive than other methods used in the literature.

The materials obtained were characterised by several techniques and showed great surfaces, great porosity, and good conductivity, which makes them promising materials for supercapacitor applications. The results showed improvement in terms of surface area (CRFZn-GO1-1661 m² g⁻¹) and specific capacitance (CRFZn-GO2-316.5 Fg⁻¹) when GO was used in the synthesis in comparison with the samples without GO, where the surface area was (CRFZn-692 m² g⁻¹), and the specific capacitance was 170.4 Fg⁻¹ (CRFZn).

The symmetric supercapacitors fabricated containing our carbon xerogel as active material demonstrated a specific capacitance of 166.6 Fg⁻¹ in 0.5 M H₂SO₄ at 0.5 Ag⁻¹ and an energy density of 14.8 Wh kg⁻¹ and a power density of 200.7 W kg⁻¹. Also, this material was employed in 1 M LiPF₆ electrolyte, which may broaden the application field of supercapacitors.

Acknowledgements

The authors are thankful for the financial support from ANPCyT (PICT 2020-01436) and CONICET (PIP 2021–2023), MinCyT Córdoba (GRTF 2018 N°27), CONICET (PIBBA 2022–2023)-Universidad Nacional de Río Cuarto (SeCyT-PPI). RCR acknowledge CONICET for a postdoctoral External Postdoctoral Fellowship (IF-2022-55992577-APN-CB#CONICET). RCR, GM, FPC, AYT and G AP, are permanent research fellows of CONICET. Also, this

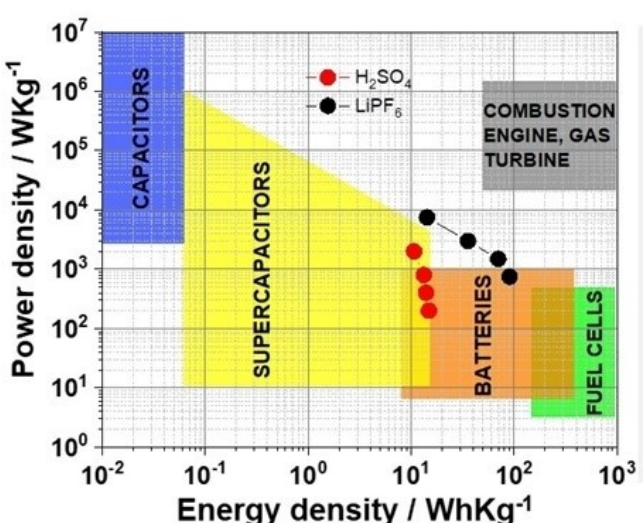


Figure 9. (a) Ragone plot of supercapacitors with CRFZn-GO1 in a carbon xerogel device in 0.5 M H₂SO₄ and 1 M LiPF₆.

research was funded by Ministerio de Ciencia e Innovación (Project PID2020-113931RB-I00 & PDC2021-120903-I00), Junta de Andalucía (FQM-175). AYT thanks to the program "Ayudas para la recualificación del sistema universitario español, Modalidad María Zambrano". The authors wish to acknowledge the technical staff from the Instituto Químico para la Energía y el Medioambiente (IQUEMA) and Servicio Central de Apoyo a la Investigación (SCAI) of Córdoba University. This work was supported by MinCyT "Iniciativa Federal para el Desarrollo de Materiales y Procesos Sustentables para el Almacenamiento de Energía, EX-2023-42139041-APNDDYGD#MCT".

Conflict of Interests

The authors declare no conflict of interest.

Data Availability Statement

The data that support the findings of this study are available from the corresponding author upon reasonable request.

Keywords: Carbon nanostructured • Xerogel • Resins • Energy storage • Supercapacitors.

- [1] Z. Liu, D. Tian, F. Shen, P. C. Nnanna, J. Hu, Y. Zeng, G. Yang, J. He, S. Deng, *J. Power Sources* **2020**, *458*, 228057.
- [2] J. Han, S. Wang, S. Zhu, C. Huang, Y. Yue, C. Mei, X. Xu, C. Xia, *ACS Appl. Mater. Interfaces* **2019**, *11*, 44624–44635.
- [3] O. Pitkänen, J. Tolvanen, I. Szenti, A. Kukovecz, J. Hannu, H. Jantunen, K. Kordas, *ACS Appl. Mater. Interfaces* **2019**, *11*, 19331–19338.
- [4] A. N. Arias, J. Villarroel-Rocha, K. Sapag, M. F. Mori, G. A. Planes, V. Flexer, A. Y. Tesio, *Carbon Trends* **2021**, *5*, 100110.
- [5] K.-S. Kim, S.-J. Park, *J. Electroanal. Chem.* **2012**, *673*, 58–64.
- [6] K. Sharma, A. Arora, S. K. Tripathi, *J. Energy Storage* **2019**, *21*, 801–825.
- [7] S. Sahoo, G. Sahoo, S. M. Jeong, C. S. Rout, *J. Energy Storage* **2022**, *53*, 105212.
- [8] J. Hou, K. Jiang, R. Wei, M. Tahir, X. Wu, M. Shen, X. Wang, C. Cao, *ACS Appl. Mater. Interfaces* **2017**, *9*, 30626–30634.
- [9] J. Ren, Y. Huang, H. Zhu, B. Zhang, H. Zhu, S. Shen, G. Tan, F. Wu, H. He, S. Lan, *Carbon Energy* **2020**, *2*, 176–202.
- [10] J. Guo, E. Lindner, *Anal. Chem.* **2009**, *81*, 130–138.
- [11] C. Zou, D. Wu, M. Li, Q. Zeng, F. Xu, Z. Huang, R. Fu, *J. Mater. Chem.* **2010**, *20*, 731–735.
- [12] P. Dibandjo, F. Chassagneux, L. Bois, C. Sigala, P. Miele, *J. Mater. Chem.* **2005**, *15*, 1917–1923.
- [13] T. Liu, L. Zhang, B. Cheng, J. Yu, *Adv. Energy Mater.* **2019**, *9*, 1803900.
- [14] A. M. Baena-Moncada, R. Coneo-Rodríguez, J. C. Calderón, J. Flórez-Montaña, C. A. Barbero, G. A. Planes, J. L. Rodríguez, E. Pastor, *Int. J. Hydrogen Energy* **2014**, *39*, 3964–3969.
- [15] M. M. Bruno, N. G. Cotella, M. C. Miras, C. A. Barbero, *Colloids Surf., A* **2010**, *362*, 28–32.
- [16] S. Zhu, N. Zhao, J. Li, X. Deng, J. Sha, C. He, *Nano Today* **2019**, *29*, 100796.
- [17] M. W. Kadi, R. M. Mohamed, A. A. Ismail, D. W. Bahnemann, *J. Colloid Interface Sci.* **2020**, *580*, 223–233.
- [18] J. Shi, H. Cui, J. Xu, N. Yan, Y. Liu, *Chem. Eng. J.* **2020**, *389*, 124459.
- [19] M. Oschatz, S. Thieme, L. Borchardt, M. R. Lohe, T. Biemelt, J. Brückner, H. Althues, S. Kaskel, *Chem. Commun.* **2013**, *49*, 5832–5834.
- [20] K. Bisaria, S. Sinha, R. Singh, H. M. N. Iqbal, *Chemosphere* **2021**, *284*, 131263.
- [21] F.-M. Chang, S. Brahma, J.-H. Huang, Z.-Z. Wu, K.-Y. Lo, *Sci. Rep.* **2019**, *9*, 905.
- [22] D. K. Sharma, S. Shukla, K. K. Sharma, V. Kumar, *Mater. Today Proc.* **2022**, *49*, 3028–3035.
- [23] B. Yan, J. Zheng, F. Wang, L. Zhao, Q. Zhang, W. Xu, S. He, *Mater. Des.* **2021**, *201*, 109518.
- [24] C. Wang, B. Yan, J. Zheng, L. Feng, Z. Chen, Q. Zhang, T. Liao, J. Chen, S. Jiang, C. Du, *Adv. Powder Mater.* **2022**, *1*, 100018.
- [25] G.-W. Liu, T.-Y. Chen, C.-H. Chung, H.-P. Lin, C.-H. Hsu, *ACS Omega* **2017**, *2*, 2106–2113.
- [26] H. Wang, S. Yu, B. Xu, *Chem. Commun.* **2016**, *52*, 11512–11515.
- [27] V. M. Gun'ko, V. M. Bogatyrov, O. I. Oranska, I. V. Urubkov, R. Leboda, B. Charmas, J. Skubiszewska-Zięba, *Appl. Surf. Sci.* **2014**, *303*, 263–271.
- [28] A. M. ElKhatat, S. A. Al-Muhtaseb, *Adv. Mater.* **2011**, *23*, 2887–2903.
- [29] O. Czakkel, K. Martti, E. Geissler, K. László, *Microporous Mesoporous Mater.* **2005**, *86*, 124–133.
- [30] C. E. I. Torres, T. E. S. Quezada, O. V. Kharissova, B. I. Kharisov, M. I. G. de la Fuente, *J. Environ. Chem. Eng.* **2021**, *9*, 104886.
- [31] F. Schipani, J. Puig, G. M. Morales, H. E. Romeo, *ACS Appl. Electron. Mater.* **2023**, *5*, 1824–1833.
- [32] H. Parsimehr, A. Ehsani, *Chem. Rec.* **2020**, *20*, 1163–1180.
- [33] F. J. Soler-Piña, C. Hernández-Rentero, A. Caballero, J. Morales, E. Rodríguez-Castellón, J. Canales-Vázquez, *Nano Res.* **2020**, *13*, 86–94.
- [34] C. Sasirekha, S. Arumugam, G. Muralidharan, *Appl. Surf. Sci.* **2018**, *449*, 521–527.
- [35] S. P. Deshmukh, D. P. Kale, S. Kar, S. R. Shirasath, B. A. Bhanvase, V. K. Saharan, S. H. Sonawane, *Nano-Struct. Nano-Objects* **2020**, *21*, 100407.
- [36] S. P. Lee, G. A. M. Ali, H. H. Hegazy, H. N. Lim, K. F. Chong, *Energy Fuels* **2021**, *35*, 4559–4569.
- [37] B. Xu, H. Wang, S. K. Yu, *Chem. Commun.* **2016**, *52*, 11512–11515.
- [38] M. Liu, F. Wei, X. Yang, S. Dong, Y. Li, X. He, *New Carbon Mater.* **2018**, *33*, 316–323.
- [39] C. Deeks, R. D. Spiops, A. Blackledge, *Lead. Edge Tech. Forensic Trace Evid. Anal. More New Trace Anal. Methods* **2022**, *1*, 67–101.
- [40] S. Tamang, S. Rai, R. Bhujel, N. K. Bhattacharyya, B. P. Swain, J. Biswas, J. Alloys Compd. **2023**, *947*, 169588.
- [41] Y. Shao, Z. Sun, Z. Tian, S. Li, G. Wu, M. Wang, X. Tong, F. Shen, Z. Xia, V. Tung, *Adv. Funct. Mater.* **2021**, *31*, 2007843.
- [42] H. Gao, Y. Ma, P. Song, J. Leng, Q. Wang, *J. Mater. Sci. Mater. Electron.* **2021**, *32*, 10058–10069.
- [43] X. Zhang, J. Qin, R. Hao, L. Wang, X. Shen, R. Yu, S. Limpanart, M. Ma, R. Liu, *J. Phys. Chem. C* **2015**, *119*, 20544–20554.
- [44] M. Kong, X. Liu, Z. Jia, B. Wang, X. Wu, G. Wu, *J. Colloid Interface Sci.* **2021**, *604*, 39–51.
- [45] B.-S. An, Y. Kwon, J.-S. Oh, C. Lee, S. Choi, H. Kim, M. Lee, S. Pae, C.-W. Yang, *ACS Appl. Mater. Interfaces* **2019**, *12*, 3104–3113.
- [46] V. Thapliyal, M. E. Alabdulkarim, D. R. Whelan, B. Mainali, J. L. Maxwell, *Diam. Relat. Mater.* **2022**, *127*, 109180.
- [47] A. Bengtsson, P. Hecht, J. Sommertunge, M. Ek, M. Sedin, E. Sjöholm, *ACS Sustain. Chem. Eng.* **2020**, *8*, 6826–6833.
- [48] E. Y. L. Teo, L. Munianandy, E.-P. Ng, F. Adam, A. R. Mohamed, R. Jose, K. F. Chong, *Electrochim. Acta* **2016**, *192*, 110–119.
- [49] A. M. Rodriguez, P. V. Jiménez, *Thermochim. Acta* **1984**, *78*, 113–122.
- [50] M. M. Gaikwad, M. Kakunuri, C. S. Sharma, *Mater. Today Commun.* **2019**, *20*, 100569.
- [51] R. da Cunha, W. V. F. do Carmo Batista, H. L. de Oliveira, A. C. dos Santos, P. M. dos Reis, K. B. Borges, P. B. Martelli, C. A. Furtado, H. de Fátima Gorogulho, *J. Photochem. Photobiol. A* **2021**, *412*, 113248.
- [52] M. Canal-Rodríguez, A. Arenillas, N. Rey-Raap, G. Ramos-Fernández, I. Martín-Gullón, J. A. Menéndez, *Carbon* **2017**, *118*, 291–298.
- [53] M. Salihovic, N. Hüsing, J. Bernardi, V. Presser, M. S. Elsaesser, *RSC Adv.* **2018**, *8*, 27326–27331.
- [54] Y. Zhang, S. Wang, P. Tang, Z. Zhao, Z. Xu, Z.-Z. Yu, H.-B. Zhang, *ACS Nano* **2022**, *16*, 8869–8880.
- [55] Y. Zhang, C. Wu, S. Dai, L. Liu, H. Zhang, W. Shen, W. Sun, C. M. Li, *J. Colloid Interface Sci.* **2022**, *606*, 817–825.
- [56] S. Aderyani, P. Flouda, S. A. Shah, M. J. Green, J. L. Lutkenhaus, H. Ardebili, *Electrochim. Acta* **2021**, *390*, 138822.
- [57] G. Xiong, P. He, Z. Lyu, T. Chen, B. Huang, L. Chen, T. S. Fisher, *Nat. Commun.* **2018**, *9*, 1–11.
- [58] A. Ray, A. Roy, S. Saha, M. Ghosh, S. Roy Chowdhury, T. Maiyalagan, S. K. Bhattacharya, S. Das, *Langmuir* **2019**, *35*, 8257–8267.
- [59] V. S. Bhat, A. Toghan, G. Hegde, R. S. Varma, *J. Energy Storage* **2022**, *52*, 104776.
- [60] Q. Zhang, C. Chen, W. Chen, G. Pastel, X. Guo, S. Liu, Q. Wang, Y. Liu, J. Li, H. Yu, *ACS Appl. Mater. Interfaces* **2019**, *11*, 5919–5927.
- [61] S. Huo, X. Zhang, B. Liang, Y. Zhao, K. Li, *J. Power Sources* **2020**, *450*, 227612.

- [62] L. Chai, P. Wang, X. Liu, Y. Sun, X. Li, J. Pan, *J. Power Sources* **2022**, *532*, 231324.
- [63] A. Daraghmeh, S. Hussain, I. Saadeddin, L. Servera, E. Xuriguera, A. Cornet, A. Cirera, *Nanoscale Res. Lett.* **2017**, *12*, 1–10.
- [64] D. T. L. Galhena, B. C. Bayer, S. Hofmann, G. A. J. Amaralunga, *ACS Nano* **2016**, *10*, 747–754.
- [65] R. A. Ponzi, R. Coneo-Rodríguez, T. M. Mondino, M. S. Moreno, G. Á. Planes, *J. Solid State Electrochem.* **2023**, *28*, 1–11.
- [66] X. Yang, Z. Jiang, B. Fei, J. Ma, X. Liu, *Electrochim. Acta* **2018**, *282*, 813–821.
- [67] H. Zhang, P. Zong, M. Chen, H. Jin, Y. Bai, S. Li, F. Ma, H. Xu, K. Lian, *ACS Nano* **2019**, *13*, 3054–3062.
- [68] S. Kumar, G. Saeed, L. Zhu, K. N. Hui, N. H. Kim, J. H. Lee, *Chem. Eng. J.* **2021**, *403*, 126352.
- [69] S.-W. Zhang, B.-S. Yin, X.-X. Liu, D.-M. Gu, H. Gong, Z.-B. Wang, *Nano Energy* **2019**, *59*, 41–49.
- [70] C. Xiong, Y. Zhang, Y. Ni, *J. Power Sources* **2023**, *560*, 232698.
- [71] I. Cameán, B. Lobato, N. Cuesta, A. B. García, *Batteries Supercaps* **2024**, *7*, e202300508.
- [72] J. P. Baboo, S. Babar, D. Kale, C. Lekakou, G. M. Laudone, *Nanomaterials* **2021**, *11*, 2899.
- [73] Z. Chen, X. Wang, Z. Ding, Q. Wei, Z. Wang, X. Yang, J. Qiu, *ChemSusChem* **2019**, *12*, 5099–5110.
- [74] L. Xie, G. Sun, F. Su, X. Guo, Q. Kong, X. Li, X. Huang, L. Wan, K. Li, C. Lv, *J. Mater. Chem. A* **2016**, *4*, 1637–1646.
- [75] J. Lang, X. Zhang, B. Liu, R. Wang, J. Chen, X. Yan, *J. Energy Chem.* **2018**, *27*, 43–56.
- [76] Y. Wang, L. Hao, Y. Zeng, X. Cao, H. Huang, J. Liu, X. Chen, S. Wei, L. Gan, P. Yang, *J. Alloys Compd.* **2021**, *886*, 161176.
- [77] M. Mirzaeian, Q. Abbas, D. Gibson, M. Mazur, *Energy* **2019**, *173*, 809–819.
- [78] B. Sun, W. Tang, H. Xiang, W. Xu, Y. Cong, G. Yuan, H. Zhu, Q. Zhang, X. Li, *New Carbon Mater.* **2022**, *37*, 564–574.
- [79] H. Wu, J. Du, A. Chen, *J. Mater. Sci.* **2023**, *58*, 5362–5371.
- [80] A. Sanchez-Sánchez, M. T. Izquierdo, S. Mathieu, G. Medjahdi, V. Fierro, A. Celzard, *Fuel Process. Technol.* **2020**, *205*, 106427.
- [81] L. Chai, J. Song, A. Kumar, R. Miao, Y. Sun, X. Liu, G. Yasin, X. Li, J. Pan, *Adv. Mater.* **2024**, *36*, 2308989.

Manuscript received: July 23, 2024
Revised manuscript received: September 2, 2024
Accepted manuscript online: September 3, 2024
Version of record online: November 14, 2024